

# Simulation of cylindrical Poiseuille flow in multiparticle collision dynamics using explicit fluid-wall confining forces

A. Ayala-Hernandez

*Grupo de Sistemas Inteligentes, Facultad de Ingeniería,  
Universidad La Salle, Benjamín Franklin 47, 06140, D.F., México.  
e-mail: arturo.ayala@lasallistas.org.mx*

H. Híjar

*Grupo de Sistemas Inteligentes, Facultad de Ingeniería,  
Universidad La Salle, Benjamín Franklin 47, 06140, D.F., México.  
e-mail: humberto.hijar@lasallistas.org.mx*

Received 18 September 2015; accepted 3 November 2015

Multiparticle collision dynamics (MPC) is a numerical technique that has been extensively used in recent years to simulate fluids supporting hydrodynamic interactions and thermal fluctuations. In this paper, we describe a method that allows MPC fluids to be confined in cavities with a complex geometry. This method is based on the introduction of an explicit repulsive interaction between the particles of the MPC fluid and the walls of the confining cavities. We apply the proposed technique in simulations of MPC fluids confined in cylindrical channels and subjected to uniform pressure gradients. We show that our method yields the correct hydrodynamic cylindrical Poiseuille flow for stick boundary conditions. We conduct an extensive numerical analysis of the method to determine the kinematic viscosity of the simulated fluid, to study finite size effects and to establish the limits for its applicability. We conclude that this technique is reliable to simulate cylindrical Poiseuille flow for a wide range of system sizes, applied pressure gradients, and viscosities and densities of the simulated fluids.

*Keywords:* Hydrodynamic flow; multiparticle collision dynamics; fluid-solid interactions.

PACS: 47.11.Mn; 02.70.Ns; 05.20.Jj

## 1. Introduction

Multiparticle Collision Dynamics (MPC) was introduced by Malevanets and Kapral, as a method for simulating fluids that obey the Navier-Stokes equations and possess hydrodynamic fluctuations [1, 2]. It was designed as an algorithm based on particles that can be combined with usual Molecular Dynamics (MD) [3, 4]. Hybrid MD-MPC simulations are used to investigate complex systems with widely separated time scales, *e.g.* colloidal suspensions and polymer solutions [5–8]. In these cases, the dynamics of the suspended phase is followed at the microscopic scale by using MD, while MPC is used to mimic the behavior of the solvent on the hydrodynamic level [2, 5, 9–11]. MPC simulates correctly the flow around the embedded particles and gives rise to the proper hydrodynamic interactions in between them [5]. Furthermore, MPC incorporates hydrodynamic fluctuations that yield Brownian forces on the suspended particles [5, 12, 13]. Consequently, fluids simulated by MPC can be used as thermal baths supporting hydrodynamic interactions.

An excellent understanding of MPC has been achieved thanks to the analytical description that has been given of the method. Since the MPC algorithm is relatively simple, it has been possible to calculate closed expressions for the transport coefficients of MPC fluids in terms of the independent simulation parameters. In particular, explicit expressions for the viscosity and thermal conductivity of MPC fluids have been obtained from projection operator methods [14–16], as

well as from kinetic theory models [9, 17]. In all the studied cases, the simulation results have been found to be in very good agreement with the theoretical expressions.

Up to the present day, MPC has been used to simulate colloids and polymer suspensions [2, 5, 18], polymers under flow [13, 19, 20], flow around objects [21, 22], vesicles under flow [23], particle sedimentation [24, 25], backtracking of colloidal particles [26], and tracking of colloids in steady shear flows [27–29]. Some reviews are available in the literature that describe the principles, main variations and applications of MPC [9, 13, 30].

In most of these applications, systems are considered to be unbounded and simulations are carried out using either the usual periodic boundary conditions or, in order to incorporate the presence of shear flow, Lees-Edwards boundary conditions [31]. However, increasing interest has been given to extend the applications of MPC to the simulation of fluids in restricted geometries [23, 32, 33]. This extension would allow, *e.g.*, to simulate some of the afore mentioned systems confined in microscopic porous or channels. So far, confined MPC fluids have been simulated by including the presence of *hard walls*, that simply reflect the incoming fluid particles back into the bulk system. Such hard walls are incorporated through the application of the so-called bounce-back boundary conditions [1]. Variations of this method that also use bounce-back rules, have been recently proposed, *e.g.* the so-called stochastic and mixed boundary conditions [24, 32, 34]. A comparison of the performance of such implementations

can be found in Ref. [34]. In simple geometries, *e.g.*, fluids confined by large plane walls, bounce-back conditions are easy to implement. However, they must be applied carefully in more complicated situations. For instance, in order to simulate particles close to corners or small features, it could be necessary to reduce considerably the simulation time step. If, in addition, particles interact with multiple surfaces during a single time step, it could be necessary to apply the bounce-back rules iteratively [34].

In this paper, we follow an alternative approach in which boundary conditions in MPC are produced by incorporating physical walls that exert explicit forces on the particles of the fluid. Our approach could be preferable to those based on hard walls in some special cases, *e.g.*, when the confining walls have a curvature such that iterative applications of the bounce-back rules are required. The explicit form of the forces to be used in our simulations is obtained from the assumption that the constraining walls are constituted by a continuous surface distribution of particles that interact with the MPC particles through a repulsive potential. The performance of our method will be studied in simulations of MPC fluids confined in a cylindrical channel and in the presence of a uniform external pressure gradient that generates the well known cylindrical Poiseuille flow. Some difficulties that are present in simulations of MPC fluids with boundary conditions of the hard wall type, in particular, the need for incorporating virtual fluid particles [33] and the problem of removing partial slip at the confining walls [34], are also encountered in our implementation. Through this paper we will carefully discuss how our method can be used to reproduce the velocity profile expected from hydrodynamics with no slip boundary conditions.

This paper is organized as follows. In Sec. 2, we will present a theoretical description of the problem of confining an MPC fluid by means of physical walls. We will obtain a mathematical expression for the fluid-wall interaction. In Sec. 3, we will discuss in detail how the theoretical framework is translated into MPC simulations. Special attention will be paid to discuss how the derived fluid-wall forces can be implemented in simulations of rough surfaces. Subsequently, in Sec. 4 we will present the results obtained from a large number of numerical experiments of cylindrical Poiseuille flow. These experiments will allow us to obtain empirically the viscosity of the confined fluids. In addition, we will study finite-size effects and determine the range of applicability of the simulation method. Finally, in Sec. 5 we will state our conclusions, and summarize the advantages and limitations of our approach.

## 2. Fluid-wall interaction

MPC fluids consist of point particles with mass  $m$ . The positions and velocities of these particles are continuous functions of time that will be represented here with the symbols  $\vec{R}_i$  and  $\vec{v}_i$ , respectively, for  $i = 1, 2, \dots, \mathcal{N}$ , where  $\mathcal{N}$  is the total number of fluid particles. In Fig. 1, we schematically illustrate some MPC particles moving close to a physical wall consisting of a continuous surface distribution of particles. Wall particles and MPC particles will be considered to interact through a repulsive potential. Specifically, if  $\vec{R}'$  represents the position of a wall particle (see Fig. 1), the energy associated with its interaction with the fluid particle at  $\vec{R}_i$ , will be given by the generalized Weeks-Chandler-Andersen (WCA) potential [35]

$$\phi(\vec{R}_i, \vec{R}') = \begin{cases} \epsilon \left[ \left( \frac{\sigma}{|\vec{R}_i - \vec{R}'|} \right)^{12n} - \left( \frac{\sigma}{|\vec{R}_i - \vec{R}'|} \right)^{6n} + \frac{1}{4} \right], & \text{if } |\vec{R}_i - \vec{R}'| < \bar{\sigma}, \\ 0, & \text{otherwise,} \end{cases} \quad (1)$$

where  $\epsilon$  is the interaction strength,  $n$  is a positive integer,  $\sigma$  is the effective diameter of the interaction, and  $\bar{\sigma} = 2^{1/6n}\sigma$  is the cutoff distance represented by the circles around the wall particles in Fig. 1. It should be noticed that the use of the WCA potential as the basic expression that will allow us to describe the effects of a solid wall on the MPC fluid, is indeed inspired in previous studies of colloids, where such potential has been used for simulating the interaction of MPC fluids with solid suspended particles [1, 5, 7, 27–29].

Let  $\rho_S$  be the numerical surface density of particles in the wall, which hereafter will be assumed to be uniform. Then, the total potential at position  $\vec{R}_i$  will be

$$\Phi(\vec{R}_i) = \rho_S \int_{S^*} dS' \phi(\vec{R}_i, \vec{R}'), \quad (2)$$

where  $S^*$  denotes the set of all those points at the surface wall satisfying the condition  $|\vec{R}_i - \vec{R}'| < \bar{\sigma}$ .

Provided that the wall surface has no abrupt changes, *i.e.*, that its curvature is not significant in comparison with the interaction radius, the integral in the right hand side of Eq. (2) can be approximated by the mean value  $\Phi(\vec{R}_i) \simeq \rho_S S^* \phi(\vec{R}_i, \vec{R}^*)$ , where  $\vec{R}^*$  is the closest point of the surface to the fluid particle. Notice that  $\vec{R}^*$  is indeed a function of  $\vec{R}_i$ , and that the geometry of the wall determines the specific form of this function. In the same limiting case,  $S^*$  can be approximated at first order as the cross section resulting from the intersection of a solid sphere of radius  $\bar{\sigma}$  with a plane located at a distance  $|\vec{R}_i - \vec{R}^*|$  from its center, *i.e.*,  $S^* \simeq \pi(\bar{\sigma}^2 - |\vec{R}_i - \vec{R}^*|^2)$ . Using these approximations the interaction potential between the wall and the MPC particle located at  $\vec{R}_i$ , takes the form

$$\Phi(\vec{R}_i) = \begin{cases} \pi\epsilon\rho_S \left( \tilde{\sigma}^2 - |\vec{R}_i - \vec{R}^*|^2 \right) \left[ \left( \frac{\sigma}{|\vec{R}_i - \vec{R}^*|} \right)^{12n} - \left( \frac{\sigma}{|\vec{R}_i - \vec{R}^*|} \right)^{6n} + \frac{1}{4} \right], & \text{if } |\vec{R}_i - \vec{R}^*| < \tilde{\sigma} \\ 0, & \text{otherwise,} \end{cases} \quad (3)$$

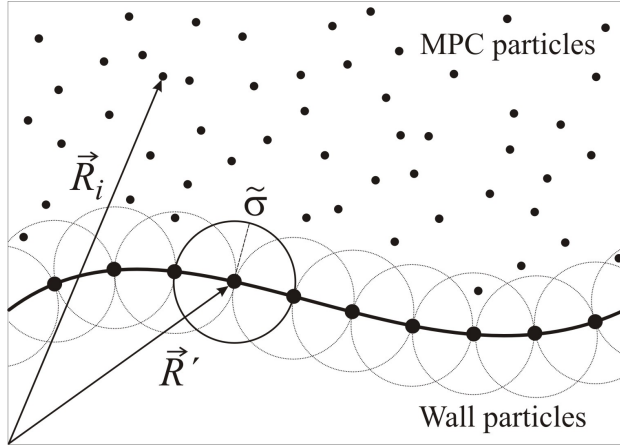


FIGURE 1. Schematic illustration of MPC particles (small circles) moving close to a physical wall (black broad curve). The latter consists of a surface distribution of particles. Vectors  $\vec{R}_i$  and  $\vec{R}'$  represent, respectively, the position of an MPC and a wall particle. The diameter of the interaction between fluid and wall particles is  $\tilde{\sigma}$ .

and the force exerted by the wall on the MPC particle,  $\vec{F}(\vec{R}_i) = -\vec{\nabla}\Phi$ , can be written as

$$\vec{F}(\vec{R}_i) = -2 \frac{d\Phi}{d|\vec{R}_i - \vec{R}^*|^2} \left[ \left( \vec{R}_i - \vec{R}^* \right) - (x_i - x^*) \vec{\nabla}x^* - (y_i - y^*) \vec{\nabla}y^* - (z_i - z^*) \vec{\nabla}z^* \right], \quad (4)$$

which is, indeed, a continuous function of  $\vec{R}_i$ .

In the previous expression, the term proportional to  $\vec{R}_i - \vec{R}^*$ , represents the force exerted by a plane surface on the fluid particle at  $\vec{R}_i$ , while the terms involving the derivatives  $\vec{\nabla}x^*$ ,  $\vec{\nabla}y^*$ , and  $\vec{\nabla}z^*$ , represent contributions arising from the curvature of the wall. When the latter is not significant, *i.e.*, when the curvature radius of the wall is much larger than the interaction diameter  $\tilde{\sigma}$ , those terms in Eq. (4) involving space derivatives of the components of  $\vec{R}^*$  can be neglected in comparison with the term  $\vec{R}_i - \vec{R}^*$ , and Eq. (4) reduces to

$$\vec{F}(\vec{R}_i) = -2 \frac{d\Phi}{d|\vec{R}_i - \vec{R}^*|^2} \left( \vec{R}_i - \vec{R}^* \right). \quad (5)$$

In this approximation, the MPC particles are assumed to interact with a wall that at the local level is a plane whose normal points along  $\vec{R}_i - \vec{R}^*$ . Although Eq. (4) is, in fact, more general than Eq. (5), it is important to notice that for the specific case of a cylindrical wall to be studied in this paper, these two expressions coincide. This can be verified by noticing that in this case  $x^* = R_0 x_i / r_i$ ,  $y^* = R_0 y_i / r_i$ ,

and  $z^* = z_i$ , where  $R_0$  is the radius of the cavity and  $r_i = (x_i^2 + y_i^2)^{1/2}$ . It is worth mentioning that Eqs. (4) and (5) represent purely repulsive conservative forces. Thus, when they are applied, the confining wall acts as a smooth surface, because any incoming fluid particle is reflected back into the bulk system with reversed momentum along the normal vector, but unchanged tangential momentum. Consequently, if the confining wall has no irregularities, Eqs. (4) and (5) can be used to simulate only surfaces with slip boundary conditions [32, 36, 37]. It has been shown in Refs. 36 and 37 that rough surfaces can be simulated by including a tangential component of the force. With this purpose, forces given by Eqs. (4) or (5), are applied in the opposite direction to that of the velocities of the incoming particles. This method is equivalent to produce local imperfections in the confining wall. With this modification, the MPC particles that come into the region of interaction with the wall, face local barriers whose orientations depend on the velocities of the particles themselves. In this new scheme, the confining wall is replaced by the surface defining the interaction region and the force applied on the incoming particles is calculated from

$$\vec{F} = -F(\vec{R}_i) \hat{v}_{\text{in}}, \quad (6)$$

where  $F(\vec{R}_i)$  is the magnitude of the force given by Eqs. (3) and (4), or (5), and  $\hat{v}_{\text{in}}$  is the unitary vector in the direction of the incoming velocity. It should be remarked that since forces given by Eqs. (4) and (5) are conservative, the velocities of the particles after the interaction with the wall will have the same magnitude than the incoming velocities, but opposite direction. Thus, this procedure will yield similar results to those given by the use the simple bounce-back rule in hard-wall methods, where surfaces with partial slip are simulated. Therefore, with the purpose of obtaining fluid-wall interactions with no slip boundary conditions, it is necessary to incorporate in the simulation scheme a procedure for increasing the tangential stress at the surface. In Ref. 37, this has been done by explicitly including forces parallel to the confining walls. Here, we will follow an alternative approach, by applying wall forces just as they are given by Eq. (6), and allowing the extra needed tangential stress to be incorporated during the collision step with virtual MPC particles, which will be described in detail in the following section.

### 3. MPC algorithm for simulation of cylindrical Poiseuille flow

We conducted a series of simulations in which, under studied conditions, the resulting behavior of the flow was found to

be steady and isothermal. We considered a total of  $\mathcal{N}$  MPC point particles of mass  $m$ , confined in a cylindrical channel of radius  $R_0$ . The long axis of this channel coincides with the  $z$  axis of a Cartesian reference frame. In the following,  $L_z$  will represent the length of the cylinder. In order to suit this geometry to the requirements of the MPC algorithm,  $R_0$  and  $L_z$  were chosen as  $R_0 = n_r a$ , and  $L_z = n_z a$ , respectively, where both  $n_r$  and  $n_z$  are integers, and  $a$  is the unitary distance. The boundary particles that conformed the confining wall, were distributed along the cylinder, at a radial distance  $R_0 + \tilde{\sigma}$ . In this manner, the set of MPC particles that do not interact with the wall particles, occupied a total volume  $\pi R_0^2 L_z$ . Finally, an external uniform axial pressure gradient with magnitude  $P'$ , was considered to exert a force on each fluid particle inside this volume.

The fluid evolved in time according to a hybrid scheme combining MD and MPC. The former allowed us to simulate the detailed motion of the fluid particles and took care of their interaction with the confining wall. The latter considered the interaction between the fluid particles in a coarse-grained fashion allowing us to incorporate collective hydrodynamic effects. Due to the presence of the confining cavity, our simulation scheme had particular features differing from usual implementations of MPC that will be discussed in detail now.

It should be remembered that typical MD-MPC simulations proceed in two main steps, commonly referred as the streaming and collision steps. During streaming, the positions and velocities of the MPC particles are updated according to the velocity Störmer-Verlet scheme, applied on a short time step of size  $\Delta t_{\text{MD}}$  [4]. Thus, if vectors  $\vec{R}_i$  and  $\vec{v}_i$ , for  $i = 1, 2, \dots, \mathcal{N}$ , represent the positions and velocities of the MPC particles, respectively, we have

$$\vec{R}_i(t + \Delta t_{\text{MD}}) = \vec{R}_i(t) + \Delta t_{\text{MD}} \vec{v}_i(t) + \frac{(\Delta t_{\text{MD}})^2}{2m} \vec{F}_i(t), \quad (7)$$

and

$$\vec{v}_i(t + \Delta t_{\text{MD}}) = \vec{v}_i(t) + \frac{\Delta t_{\text{MD}}}{2m} \left[ \vec{F}_i(t + \Delta t_{\text{MD}}) + \vec{F}_i(t) \right], \quad (8)$$

where  $\vec{F}_i$  denotes the total force on the  $i$ th particle, *i.e.*, the sum of the external pressure gradient and the confining forces. In order to calculate the latter, we applied Eqs. (3) and (5) where the quantities  $\hat{v}_{\text{in}}$  and  $\vec{R}^*$  were numerically determined according to the procedure illustrated in Fig. 2. There, we show an MPC particle located in the bulk system at time  $t - \Delta t_{\text{MD}}$ , which is observed to get into the interaction region at time  $t$ . First, the velocity of such particle is approximated as the difference,  $\vec{v}_i(t) = (\vec{R}_i(t) - \vec{R}_i(t - \Delta t_{\text{MD}})) / \Delta t_{\text{MD}}$ , from which the direction of the force can be determined as  $\hat{v}_{\text{in}} = \vec{v}_i(t) / |\vec{v}_i(t)|$ .

On the other hand,  $\vec{R}^*$  can be written in the form  $\vec{R}^* = \vec{R}_p + \tilde{\sigma} \hat{v}_{\text{in}}$ , where  $\vec{R}_p$  denotes the point where the par-

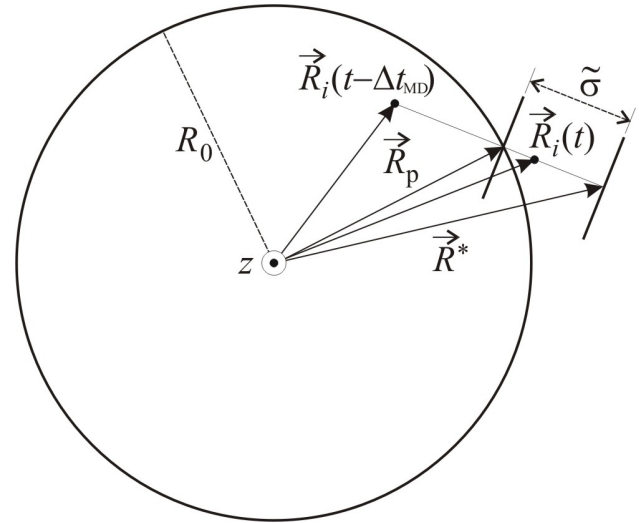


FIGURE 2. Quantities used to calculate the force exerted by the confining cylindrical surface and the fluid particles.

ticle crosses the interaction surface, which is written as  $\vec{R}_p = h(\vec{R}_i(t) - \vec{R}_i(t - \Delta t_{\text{MD}}))$ . Finally, the factor  $h$  in the last equality is determined from the condition that  $\vec{R}_p$  is a point of the cylindrical surface, *i.e.*  $R_{p,x}^2 + R_{p,y}^2 = R_0^2$ .

The characteristic collision step of MPC was applied periodically after performing  $n_{\text{MD}}$  MD integration steps, *i.e.*, at time intervals of size  $\Delta t = n_{\text{MD}} \Delta t_{\text{MD}}$ , where  $n_{\text{MD}}$  is an integer. The collision step required to subdivide the simulation box in cells of volume  $a^3$ , where interparticle collisions were simulated. With this purpose, the center of mass velocity of each cell was calculated and particles within the same cell were forced to exchange their velocities according to

$$\vec{v}'_i = \vec{v}_{\text{c.m.}} + \mathbf{R}(\alpha; \hat{n}) \cdot [\vec{v}_i - \vec{v}_{\text{c.m.}}], \quad (9)$$

where  $\vec{v}'_i$  and  $\vec{v}_i$  denote the velocities of the  $i$ th particle after and before collision, respectively;  $\vec{v}_{\text{c.m.}}$  the center of mass velocity of the cell; and  $\mathbf{R}(\alpha; \hat{n})$  a stochastic rotation matrix, which rotates velocities by an angle  $\alpha$  around a random axis  $\hat{n}$ . It is worth stressing that  $\alpha$  is a parameter whose value is fixed through the whole simulation, while  $\hat{n}$  is sampled in each cell at every collision step by randomly selecting a point on the surface of a sphere with unit radius. It was noticed by Ihle and Kroll that the presence of collision cells introduce an artificially fixed frame of reference, which breaks the property of Galilean invariance and leads to a breakdown of the molecular chaos assumption [15,16]. Thus, in order to restore this property, a uniform random displacement of the cells should be implemented, before collisions take place [15,16].

In the presence of confining surfaces, both the division of the system into cells and the subsequent random displacement of these cells, must be implemented with caution. The reason is that cells near the surfaces might be partially empty and collisions inside them might take place as in a fluid with lower density, thus yielding different physical properties than in the interior cells [33]. This problem could be solved by introducing *virtual particles* that fill the partially empty

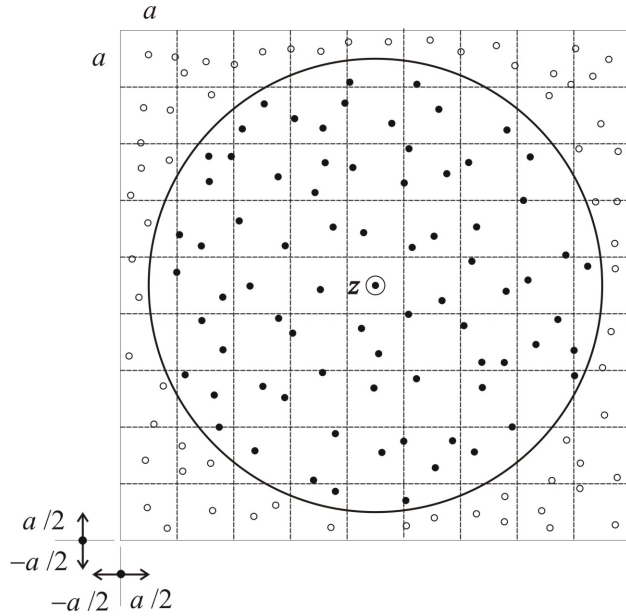


FIGURE 3. Schematic illustration of the procedure used to introduce virtual particles. The system is extended to a prism of volume  $(2n_x + 1)(2n_y + 1)n_z a^3$ , and the space left by real particles (black filled circles) is filled with virtual particles (empty circles). Virtual particles are introduced at random positions in the empty space. The number of virtual particles is chosen such that the density is continuous over the whole extended system.

cells and help collisions to be performed at the right average density. In order to introduce virtual particles in our simulations, we followed the procedure schematically shown in Fig. 3. First, we extended the system to a rectangular prism with volume  $(2n_x + 1)(2n_y + 1)n_z a^3$ . Then, the space outside the cylindrical cavity was filled with virtual particles of mass  $m$ . Virtual particles were uniformly distributed in the space outside the cylinder using a Monte Carlo sampling scheme. In this work, we decided to incorporate the virtual particles with velocities selected according to two different schemes, hereafter referred as the simulation schemes I and II.

In scheme I, the velocity of each virtual particle was sampled from a Gaussian distribution with zero mean and the standard deviation dictated by the equipartition law. We will show in Sec. 4 that this procedure yields flow inside the cylinder with partial slip boundary conditions.

In the simulation scheme II, we calculated first the center of mass velocity of the bulk particles enclosed in the region between the radii  $R_0 - a/2$  and  $R_0$ . As it could be expected, this average velocity was found to vanish in the  $x$  and  $y$  direction, but to be different from zero,  $\bar{v}$ , along the  $z$  axis. Then, virtual particles were introduced with velocities taken from a Gaussian distribution with the same standard deviation as in scheme I, centered at the velocity  $(0, 0, -\kappa\bar{v})$ . The quantity  $\kappa$  will be considered an adjustable parameter and, indeed, it will be shown in Sec. 4 that it can be tuned to obtain simulations of flow with stick boundary conditions.

At this point it is convenient to notice that spatially unrestricted MPC fluids have a total kinematic viscosity that can be written in the form  $\nu = \nu^{\text{col}} + \nu^{\text{kin}}$ , where  $\nu^{\text{col}}$  and

$\nu^{\text{kin}}$  represent contributions due to the streaming (kinetic) and collisional steps of MPC, respectively. In terms of the independent simulation parameters these quantities read as

$$\nu^{\text{col}} = \frac{a^2}{18N\Delta t} (N - 1 + e^{-N}) (1 - \cos(\alpha)), \quad (10)$$

$$\nu^{\text{kin}} = \frac{k_B T \Delta t}{2m} \times \left[ \frac{5N}{(N-1+e^{-N})(2-\cos(\alpha)-\cos(2\alpha))} - 1 \right], \quad (11)$$

respectively, where  $N$  is the numerical density of MPC particles,  $k_B$  is the Boltzmann constant, and  $T$  is the temperature of the simulated fluid. In the case of our implementation, in which the MPC fluid is confined, the stress tensor should have contributions arising from the interaction with the wall and from the collision with the virtual particles. The former should modify the kinetic viscosity coefficient, while the latter should change the collisional viscosity of the fluid.

The precise form of the changes in the viscosity of the MPC fluid induced by confinement, could be obtained from a kinetic model similar to the one that has been carried out in Ref. 33 for the case of a fluid confined between two parallel plates. In this paper we will follow an alternative approach and obtain the viscosity of the confined fluid empirically from the results of our numerical experiments. We will show that corrections to Eqs. (10) and (11), due to interaction with the wall and collisions with the virtual particles are small indeed.

In addition, it is important to mention that particles interacting with the cylindrical confining wall, i.e. those with  $x$  and  $y$  coordinates satisfying  $x^2 + y^2 > R_0^2$ , were excluded from participation in the collision step, since their trajectories would be deflected by collisions and they would escape from the simulation box through the confining walls.

We implemented periodic boundary conditions along the  $z$  axis. In addition, in order to prevent viscous heating of the simulated system under flow, we applied a thermostatting procedure after each collision step. This thermostat was based on a local velocity rescale that fixed the temperature of the system at the value  $T$  [27–29].

Numerical experiments were performed by sorting the MPC particles into the cylindrical cavity with uniformly distributed random positions and velocities. No initial overlapping existed between the fluid particles and the confining surface, the total momentum of the system was fixed to zero, and its total energy was adjusted to the value dictated by the equipartition law at temperature  $T$ . Then, the hybrid MD-MPC algorithm was applied to the ensemble of fluid particles subjected to the external field  $P'$  and to the constraining surface forces. This thermalization process was applied over  $10^5$  steps of the MD-MPC algorithm after which we observed that the proper distribution of velocities and hydrodynamic fields were established. Finally, a simulation stage was conducted over  $2 \times 10^5$  steps, that allowed us to calculate the stationary hydrodynamic fields in the system. In this work, we will

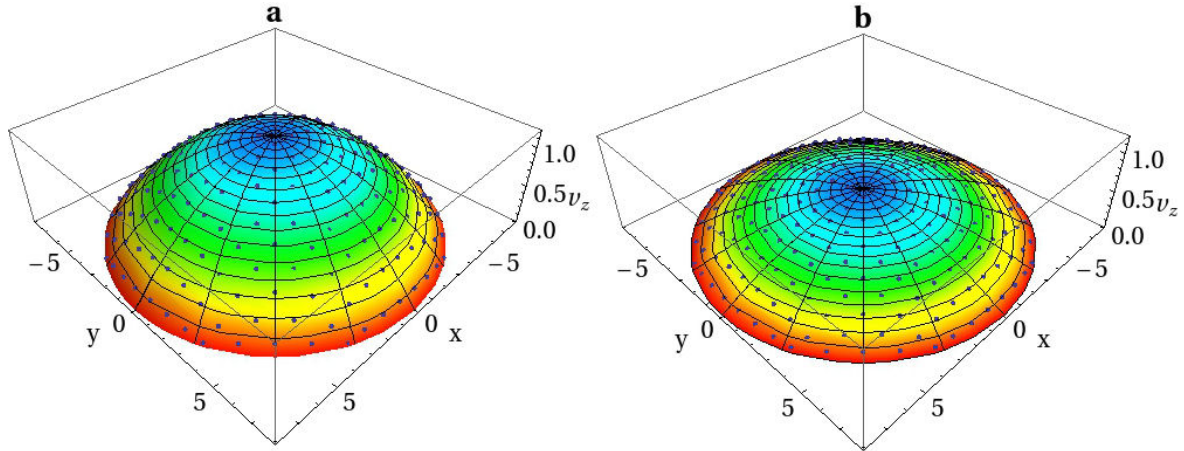


FIGURE 4. Velocity profiles obtained from simulations of confined MPC fluids in a cylindrical cavity, performed according with scheme I at collision angles  $\alpha = 15^\circ$ , **a**, and  $\alpha = 180^\circ$ , **b**. Symbols correspond to numerical results while continuous surfaces have been obtained from a least squares fit based on Eq. (12).

restrict the analysis to the study of the velocity field which will be calculated as the time average of the center of mass velocity of the MPC collision cells.

The independent parameters of the simulations were the length of the MPC cells,  $a$ ; the time-step between MPC collisions,  $\Delta t$ ; the average number of particles per cell,  $N$ ; the thermal energy,  $k_B T$ ; the MPC rotation angle,  $\alpha$ ; and the mass of the individual MPC particles,  $m$ . All our simulations were performed by fixing these parameters at  $a = 1$ ,  $k_B T = 1$ ,  $\Delta t = 0.05$ , and  $m = 1$ . Notice that here, as well in the rest of the paper, we will use simulation units (s.u.) instead of physical units. The parameters characterizing the interaction between the particles and the confining walls were chosen as  $\epsilon = k_B T/2$ ,  $\sigma = a/2$ , and  $\rho_S = 1/2a^2$ . The MD time-step was chosen as  $\Delta t_{MD} = 0.005$ , for which no instabilities of the simulations were observed.

## 4. Results

We shall present here the results obtained from the application of the algorithm described in Sec. 3. First, in Sec. 4.1, we will present the results obtained from the simulation scheme I, in which virtual particles are introduced with zero mean velocity, and show that this scheme yields cylindrical Poiseuille flow with partial slip boundary conditions. Afterwards, in Sec. 4.2, we will describe how this method can be modified by introducing virtual particles with nonzero mean velocity (simulation scheme II), in order to simulate flow with stick boundary conditions.

### 4.1. Simulation of cylindrical Poiseuille flow with slip boundary conditions

The velocity profile expected for the simulation geometry introduced in Sec. 3, is the classical cylindrical Poiseuille flow [38], which can be written in the form

$$v_z(x, y) = v_0 + \frac{P'}{4\rho\nu} (R_0^2 - r^2), \quad (12)$$

where  $v_0$  is the velocity at the boundary surface,  $\nu$  is the kinematic viscosity of the fluid, and  $r = (x^2 + y^2)^{1/2}$ , is the radial polar coordinate. Due to the symmetry of the system, velocity components in the  $x$  and  $y$  directions vanish, *i.e.*,  $v_x = v_y = 0$ . These equations, together with the condition of uniform density and temperature, are the solutions of the hydrodynamic equations for a viscous fluid moving through a cylinder due to the pressure gradient  $P'$ , and kept at constant temperature by an external thermostat.

As a first result, we notice that our numerical implementation produces flows that can be very well adjusted by Eq. (12). In order to illustrate the validity of this assertion, we present the results from a first series of experiments for MPC fluids confined in a cylinder with fixed size defined by  $R_0 = 8a$ , and  $L_z = 32a$ . The numerical experiments were carried out with a total number of 16384 MPC particles acted by a pressure gradient of magnitude  $P' = 0.4$ . We performed simulations varying the MPC collision angle,  $\alpha$ , at twelve different values uniformly distributed from  $15^\circ$  to  $180^\circ$ . This numerical setup was intended to test the validity of the method for small, as well as large, values of  $\alpha$ . In the former case, the simulated fluid is expected to be in the so-called gas regime, where contributions to the material properties of the fluid arising from streaming dynamics (kinetic), dominate over contributions due to collisions [9, 30]. In the opposite case, *i.e.*, when  $\alpha$  is large, the interaction between MPC particles is stronger and the fluid behaves in the so-called liquid regime, where collisional effects are larger and dominate over kinetic effects. Figures 4 a) and b) show the velocity profiles obtained for the extreme cases  $\alpha = 15^\circ$  and  $\alpha = 180^\circ$ , respectively. There, points correspond to the results from simulations while the continuous surfaces were obtained from a simple least squares fit of the results, based on Eq. (12), using  $v_0$  and  $\nu$  as the adjustable parameters.

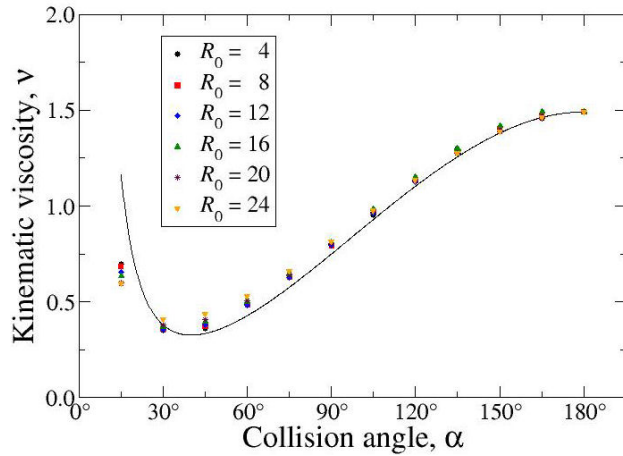


FIGURE 5. Estimated viscosity of the simulated MPC fluid confined in cylinders with different radii  $R_0$ , as function of the collision angle  $\alpha$ . Symbols represent results from numerical simulations while the continuous line corresponds to the analytical viscosity obtained from Eqs. (10) and (11).

TABLE I. Estimated values of  $v_0$  and  $\nu$  for simulations of cylindrical Poiseuille flow in MPC fluids with different collision angles,  $\alpha$ . Fluids were confined in a pipe with radius  $R_0 = 8a$ , and subjected to an external pressure gradient  $P' = 0.4$ . The complete set of remaining simulation parameters is described through the text.

Collision angle, $\alpha$	Slip velocity, $v_0$	Kinematic viscosity, $\nu$
15°	0.0126	0.692
30°	0.0019	0.361
45°	0.0309	0.379
60°	0.0399	0.489
75°	0.0337	0.639
90°	0.0292	0.805
105°	0.0267	0.987
120°	0.0223	1.146
135°	0.0220	1.303
150°	0.0201	1.422
165°	0.0180	1.486
180°	0.0178	1.510

In all the experiments of this series, the established stationary velocity profiles could be very well adjusted in this manner. In Table I, we summarize the results of the fitting procedure. There, we present the estimated values of  $v_0$  and  $\nu$  as function of the collision angle  $\alpha$ . Our results show that the scheme I simulates fluids with partial slip boundary conditions since, in general,  $v_0$  was found to be different from zero. More importantly, this procedure allowed us to obtain an empirical estimation of the viscosity of the confined MPC fluid, which is plotted in Fig. 5 as function of  $\alpha$ . In Fig. 5, we compare the results from our numerical experiments with the analytical value of the kinematic viscosity,  $\nu = \nu^{\text{col}} + \nu^{\text{kin}}$ , where

$\nu^{\text{col}}$  and  $\nu^{\text{kin}}$  are given in terms of the simulation parameters by Eqs. (10) and (11), respectively. In Fig. 5, we have also included the results from 60 additional experiments carried with the same parameters described above but in systems with different sizes defined by  $R_0 = 4, 12, 16, 20$ , and  $24$ . We notice that the numerical and theoretical results are in very good qualitative agreement. Indeed, the viscosity of the simulated systems fits very well the analytical expressions for large values of the collision angle  $\alpha \gtrsim 120^\circ$ , but exhibits deviations in simulations carried out in the gas regime. This suggests that the confining cylindrical surface modifies the kinematic viscosity of the simulated MPC fluid but has no appreciable effect on the collisional contribution.

The hydrodynamic regime corresponding to the set of simulations presented so far, can be identified more clearly in terms of the Reynolds number,  $\text{Re}$ , which, for a given flow, quantifies the relevance of the inertial forces with respect to the viscous effects. For flow in a circular pipe,  $\text{Re}$  can be defined as

$$\text{Re} = \frac{\bar{v}_z D_H}{\nu}, \quad (13)$$

where  $\bar{v}_z$  is the average flow velocity along the pipe and  $D_H = 2R_0$ , is the so-called hydraulic diameter. In our simulations,  $\bar{v}_z$  can be calculated straightforwardly allowing us to estimate the values of  $\text{Re}$  corresponding to each produced flow. It was observed that  $\text{Re}$  varied in a rather wide range of values, from  $\text{Re} = 0.3872$ , for  $\alpha = 180^\circ$  and  $R_0 = 4$ , to  $\text{Re} = 952.17$ , for  $\alpha = 30^\circ$  and  $R_0 = 24$ . Thus, we notice that our simulations covered flows with Reynolds number extending over three orders of magnitude and, since turbulence in a cylindrical pipe is expected for  $\text{Re} \simeq 2000$  [39], we conclude that our simulations were performed in the laminar flow regime.

Another dimensionless number that can be used to characterize the hydrodynamic regime is the Schmidt number,  $\text{Sc}$ , defined as  $\text{Sc} = \nu/D$ , where  $D$  is the diffusion coefficient. This quantity represents the ratio of the rate of diffusive momentum transfer to the rate of diffusive mass transfer and, therefore, indicates whether momentum transfer in a flow occurs by mass transport,  $\text{Sc} \sim 1$ , or by molecular collisions,  $\text{Sc} > 1$ . In MPC,  $D$  can be obtained in terms of the simulation parameters from the equation [30]

$$D = \frac{k_B T \Delta t}{2m} \left[ \frac{3N}{(1 - \cos(\alpha))(N - 1 + e^{-N})} - 1 \right]. \quad (14)$$

This equation, together with the estimated values of the kinematic viscosity can be used to determine the values of  $\text{Sc}$ . We found that our experiments covered flows with Schmidt numbers ranging from  $\text{Sc} = 0.2021$ , for  $\alpha = 15^\circ$ , to  $\text{Sc} = 44.7134$ , when  $\alpha = 180^\circ$ .

#### 4.2. Simulation of cylindrical Poiseuille flow with stick boundary conditions

It has been described in Sec. 3 that in the simulation scheme II, virtual particles at partially empty cells are intro-

TABLE II. Parameter  $\kappa$  estimated from simulations performed with different values of  $\alpha$ ,  $R_0$  and  $P'$ . This parameter was obtained from a steepest descendant method that stopped when simulations produced flows with velocities at the boundaries smaller that 0.001. All quantities are given in simulation units.

$P' = 0.4$					
Collision angle, $\alpha$	$R_0 = 8a$	$R_0 = 12a$	$R_0 = 16a$	$R_0 = 20a$	$R_0 = 24a$
135°	0.52	0.68	0.56	0.41	0.45
150°	0.51	0.66	0.58	0.41	0.42
165°	0.54	0.67	0.56	0.41	0.43
180°	0.53	0.67	0.56	0.41	0.41
$P' = 1.2$					
Collision angle, $\alpha$	$R_0 = 8a$	$R_0 = 12a$	$R_0 = 16a$	$R_0 = 20a$	$R_0 = 24a$
135°	0.49	0.66	0.59	0.61	0.89
150°	0.48	0.65	0.56	0.53	0.73
165°	0.48	0.64	0.55	0.49	0.64
180°	0.47	0.64	0.54	0.48	0.61

duced with a mean velocity in the  $z$  direction given by  $-\kappa\bar{v}$ , where  $\kappa \neq 0$ . The momentum exchange due to collisions between fluid particles and virtual particles close to the cylindrical wall, can be controlled by varying the value of the parameter  $\kappa$ . This helps to reduce or increase the velocity of the fluid particles near the surface and, thus, to adjust the value of the velocity field at the boundary. In this work, we adopt an empirical approach to find the values of the parameter  $\kappa$  that fit the flow velocity at the boundary,  $v_0$ , close to 0. With this purpose, we implemented a simple steepest descent procedure and, for given values of  $\alpha$ ,  $R_0$ , and  $P'$ , we carried out simulations varying  $\kappa$  in increments of size  $\Delta\kappa = \pm 0.01$ , until  $|v_0|$  was found to be smaller than an error parameter with fixed magnitude 0.001.

In a first series of experiments, we observed that  $\kappa$  exhibited strong variations for small values of the MPC collision angle, more precisely for  $\alpha \lesssim 120^\circ$ . Thus, in order to simplify the analysis, we restricted ourselves to estimate  $\kappa$  only in the case of MPC dynamics dominated by collisional effects and considered solely simulations with  $\alpha = 135^\circ, 150^\circ, 165^\circ$ , and  $180^\circ$ . The dependence of  $\kappa$  on the size of the system and the external pressure gradient was explored by performing simulations with the parameters  $R_0 = 8, 12, 16, 20$ , and  $24$ ; and  $P' = 0.4$  and  $1.2$ . This gave a total of 40 additional experiments performed to determine  $\kappa$  as function of  $\alpha$ ,  $R_0$  and  $P'$ . The results of these experiments are summarized in Table II. There, it can be seen that  $\kappa$  does not show a strong dependence on  $\alpha$  for small values of  $P'$  ( $\sim 0.4$ ), but changes considerably as function of the collision angle when  $P'$  is large ( $\sim 1.2$ ). In a first approximation, in order to obtain a simplified description of the problem, we considered  $\kappa$  to be independent of  $\alpha$ , and the resulting function  $\kappa = \kappa(R_0, P')$ , was approximated by taking the average over the results obtained at different collision angles. This procedure yielded eight numerical estimations

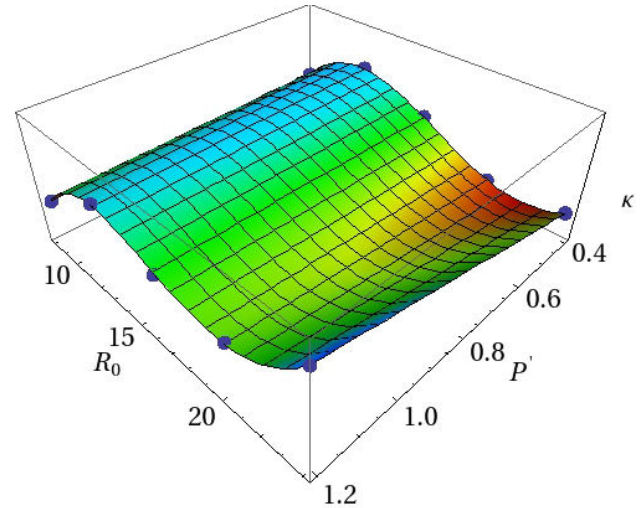


FIGURE 6. Parameter  $\kappa$  used in simulation scheme II to fix the average velocity of virtual particles as function the size of the system,  $R_0$ , and the imposed pressure gradient  $P'$ . Symbols correspond to the values obtained from simulations as they are given in Table II, after averaging over the collision angle,  $\alpha$ . The continuous surface corresponds to the fit of the experimental data represented by Eq.(16).

of  $\kappa(R_0, P')$ , which are shown as symbols in the plot of Fig. 6. There, it can be observed that the behavior of  $\kappa$  at the constant values  $P' = 0.4$ , and  $P' = 1.2$ , is very similar, and since in both cases  $\kappa$  has two local extrema with respect to  $R_0$ , it was suggested to approximate it as

$$\kappa = a_0(P') + a_1(P')R_0 + a_2(P')R_0^2 + a_3(P')R_0^3, \quad (15)$$

where the parameters  $a_i$ , for  $i = 1, 2, 3, 4$ , for fixed  $P' = 0.4$  and  $P' = 1.2$ , were obtained from a nonlinear curve fitting procedure, although their explicit values are not presented her for brevity. In the simplest case, the general functions  $a_i(P')$ , can be assumed to be linear, *i.e.*,

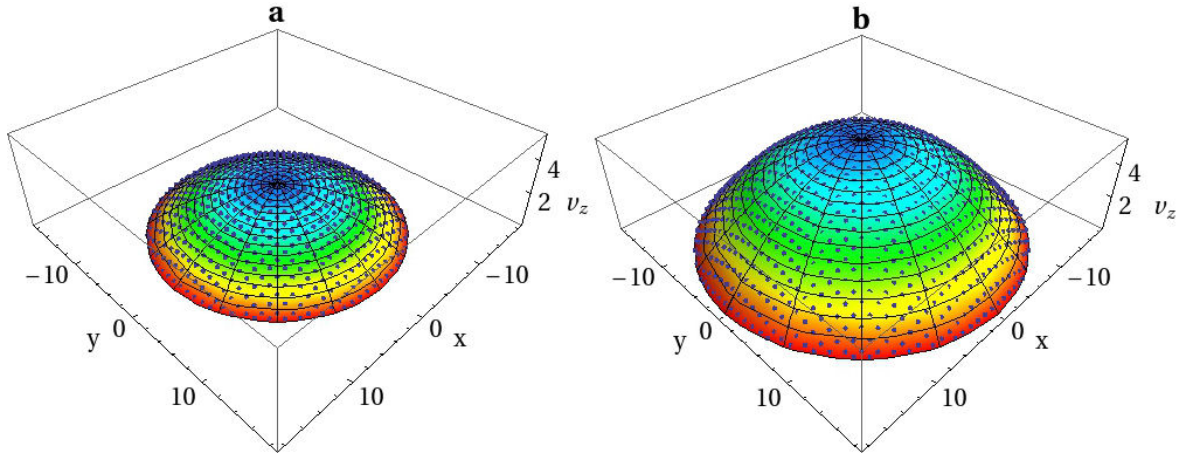


FIGURE 7. Velocity profiles obtained from simulations of confined MPC fluids in a cylindrical cavity, performed according with scheme II. Case **a** corresponds to simulation parameters  $\{\alpha = 140^\circ, R_0 = 14, P' = 0.6\}$ , while in case **b** we have used  $\{\alpha = 155^\circ, R_0 = 18, P' = 0.8\}$ . Symbols represent the numerical results while continuous surfaces correspond to the cylindrical Poiseuille flow with no slip boundary conditions.

$a_i(P') = b_i + m_i P'$ , and the values the quantities  $b_i$  and  $m_i$  can be finally obtained from those of  $a_i(0.4)$  and  $a_i(1.2)$ .

The overall result of this procedure can be summarized in the numerical approximation

$$\begin{aligned} \kappa(R_0, P') = & -1.3455 - 0.08125 P' \\ & + (0.4196 + 0.01292 P') R_0 \\ & - (0.0270 + 0.00181 P') R_0^2 \\ & + (0.0005 + 0.00009 P') R_0^3, \end{aligned} \quad (16)$$

and this function is represented as the continuous surface in Fig. 6. We stress that this function is expected to work well in the limit of large collision angles,  $\alpha \in (135^\circ, 180^\circ)$ , and moderate pressure gradients  $P' \sim 0.4$ .

In order to illustrate the applicability of this approximation, we considered three final simulations performed with the following sets of parameters  $\{\alpha = 140^\circ, R_0 = 14, P' = 0.6\}$ ,  $\{\alpha = 155^\circ, R_0 = 18, P' = 0.8\}$ , and  $\{\alpha = 170^\circ, R_0 = 22, P' = 1.0\}$ . Simulations were carried out following the simulation scheme II, where the factor  $\kappa$  that determined the velocity of the virtual particles was calculated according to Eq. (16). The three considered cases yielded cylindrical Poiseuille flows with boundary velocities  $v_0 = -1.2 \times 10^{-4}$ ,  $-1.7 \times 10^{-3}$  and 0.18, respectively. These results illustrate that the proposed method is reliable for producing flow with no slip boundary conditions in the expected range of simulation parameters. In fact, for small ( $P' = 0.4$ ), and medium pressure gradients ( $P' = 0.8$ ), the simulated flows had a velocity at the boundary surface that were just 0.006% and 0.04%, respectively, of the maximum velocity in the pipe. The velocity profiles obtained from these two simulations are presented in Figs. 7 a) and b), where they are compared with the cylindrical Poiseuille flow, Eq. (12), evaluated at  $v_0 = 0$  and  $\nu$  given by Eqs. (10) and (11). These figures show that the numerical results in the corresponding

range are in very good agreement with the expected cylindrical Poiseuille flow with no slip boundary conditions.

For large values of the imposed gradient, the flow velocity at the boundary surface was found to be 1.8% of the maximum velocity in the pipe. This deviation could be expected since Eq. (16) was obtained under the assumption that the factor  $\kappa$  was independent of  $\alpha$ , a situation that is not fulfilled in the case of large values of  $P'$ .

## 5. Discussion

We have presented a method for simulating cylindrical Poiseuille flow in MPC fluids. In this method, the pipe in which the MPC fluid is kept, is modeled as a physical barrier that interacts by means of an explicit force with the particles of the confined fluid. One important feature of the proposed model is that, starting from the microscopic details of the confinement wall, we have proposed a novel integrated equation for its interaction with the fluid that involves its geometrical properties. This feature will be exploited in subsequent publications where we will analyze MPC fluids confined in complex geometries, *e.g.*, concentric cylinders and mirror symmetric 3D channels.

The problem of confining MPC fluids by means of explicit forces presented difficulties that are also found when these fluids are confined by hard walls. Specifically, it was necessary to propose an algorithm in which the integrated scheme for the confinement force could be applied and, as well, allowed us to incorporate virtual particles at the MPC collision step and to eliminate partial slip at the surface of fluid-solid interaction.

We have used two different implementations referred as the simulation schemes I and II. In the former, virtual particles were introduced with zero mean velocity and cylindrical Poiseuille flow was found to present partial slip at the boundary. In scheme II, the velocities of the virtual particles were

adjusted to yield flow with stick boundary conditions. The approach followed to achieve this adjustment, summarized in Eq. (16), was completely empirical. This restricts the applicability of our method to the range of parameters used to derive this expression, namely, to the liquid-like regime of MPC, and to flows driven by moderate pressure gradients. However, we consider that this is an acceptable range of values, since most of current applications of MPC are carried out with parameters similar to those used in the present study. The reliability of the method was shown by performing independent simulations where slip velocity was found to be less than 1% of the maximum flow velocity.

A major issue that we have left open in this work concerns the study of the performance of our simulation method based on explicit forces, with respect to the one given by other established techniques, *e.g.*, simulation of Poiseuille flow based on the application of bounce-back rules. From the point of

view of the computational efficiency, the main difference between our method and those based on hard walls, is the cost that must be paid during the streaming step by the application of the MD integration scheme. This requires to subdivide the MPC collision time step in smaller time intervals, where forces on particles due to the presence of the wall must be calculated. Thus, it is expected that, indeed, our implementation will exhibit a lower performance than methods based on hard walls. Nevertheless, the advantage of our scheme is that it is in fact closer to simulate a real situation since confinement of fluids by solids is always mediated by interaction potentials, while hard walls are just idealizations.

## Acknowledgments

H. Híjar thanks Universidad La Salle for financial support under grant NEC-04/15.

- 
1. A. Malevanets and R. Kapral, *J. Chem. Phys.* **110** (1999) 8605.
  2. A. Malevanets and R. Kapral, *J. Chem. Phys.* **112** (2000) 7260.
  3. D. Frenkel and B. Smith, *Understanding Molecular Simulations: from Algorithms to Applications*, Academic Press, San Diego, (2002).
  4. M. Griebel, S. Knapek and G. Zumbusch, *Numerical Simulation in Molecular Dynamics. Numerics, Algorithms, Parallelization, Applications*, Springer, Berlin Heidelberg, (2007).
  5. J. T. Padding and A. A. Louis, *Phys. Rev. Lett.* **93** (2004) 220601.
  6. I. Ali, D. Marenduzzo and J. Yeomans, *J. Chem. Phys.* **121** (2004) 8635.
  7. M. Hecht, J. Harting, T. Ihle and H. J. Hermann, *Phys. Rev. E* **72** (2005) 011408.
  8. J. T. Padding and A. A. Louis, *Phys. Rev. E* **74** (2006) 031402.
  9. G. Gompper, T. Ihle, D.M. Kroll and R.G. Winkler, *Adv. Polym. Sci.* **221** (2009) 1-87.
  10. S. H. Lee and R. Kapral, *J. Chem. Phys.* **121** (2004) 11163.
  11. N. Kikuchi, J. F. Ryder, C. M. Pooley and J. M. Yeomans, *Phys. Rev. E* **71** (2005) 061804.
  12. H. Híjar and G. Sutmman, *Phys. Rev. E* **83** (2011) 046708.
  13. J. M. Yeomans, *Physica A* **369** (2006) 159.
  14. E. Tüzel, M. Strauss, T. Ihle and D. M. Kroll, *Phys. Rev. E* **68** (2003) 036701.
  15. T. Ihle and D. M. Kroll, *Phys. Rev. E* **63** (2001) 020201.
  16. T. Ihle and D. M. Kroll, *Phys. Rev. E* **67** (2003) 066706.
  17. C. M. Pooley and J. M. Yeomans, *J. Phys. Chem. B* **109** (2005) 6505.
  18. N. Kikuchi, A. Gent and J. M. Yeomans, *Eur. Phys. J. E* **9** (2002) 63.
  19. A. Malevanets and J. M. Yeomans, *Europhys. Lett.* **52** (1999) 231.
  20. M. Ripoll, K. Mussawisade, R. G. Winkler and G. Gompper, *Europhys. Lett.* **68** (2004) 106.
  21. A. Lamura, G. Gompper, T. Ihle and D. M. Kroll, *Europhys. Lett.* **56** (2001) 319.
  22. E. Allahyarov and G. Gompper, *Phys. Rev. E* **66** (2002) 036702.
  23. H. Noguchi and G. Gompper, *Phys. Rev. E* **72** (2005) 011901.
  24. A. Moncho Jordá, A. A. Louis and J. T. Padding, *Phys. Rev. Lett.* **104** (2010) 068301.
  25. A. Moncho Jordá, A. A. Louis and J. T. Padding, *J. Chem. Phys.* **136** (2012) 064517.
  26. M. Belushkin, R. G. Winkler and G. Foffi, *J. Phys. Chem. B* **115** (2011) 14263.
  27. H. Híjar, *J. Chem. Phys.* **139** (2013) 234903.
  28. J. Fernández and H. Híjar, *Rev. Mex. Fis.* **61** (2015) 1.
  29. H. Híjar, *Phys. Rev. E* **91** (2015) 022139.
  30. R. Kapral, *Adv. Chem. Phys.* **140** (2008) 89.
  31. A. W. Lees and S. F. Edwards, *J. Phys. C* **5** (1972) 1921.
  32. Y. Inoue, Y. Chen and H. Ohashi, *J. Stat. Phys.* **107** (2002) 85.
  33. R. G. Winkler and C. C. Huang, *J. Chem. Phys.* **130** (2009) 074907.
  34. J.K. Withmer and E. Luijten, *J. Phys.: Condens. Matter*, **22** (2010) 104106
  35. J.P. Hansen and I.R. McDonald, *Theory of simple liquids*, 2nd ed. Academic Press, London, (1986).
  36. A. Ayala-Hernandez and H. Híjar, *International Journal of Mathematical, Computational, Physical and Quantum Engineering* **8** (2014)
  37. A. Ayala-Hernandez and H. Híjar, *Revista del Centro de Investigación. Universidad La Salle* (2015) (submitted)
  38. L.D. Landau and E.M. Lifshitz, *Fluid Mechanics*, 2nd revised English version, Pergamon, London (1959).
  39. K. Avila, D. Moxey, A. de Lozar, M. Avila, D. Barkley and B. Hof, *Science* **333** (2011) 192.